Journal of Molecular Structure: THEOCHEM 958 (2010) 82–91

Contents lists available at ScienceDirect

Journal of Molecular Structure: THEOCHEM

journal homepage: www.elsevier.com/locate/theochem

Theoretical investigation of the reaction mechanism of atomic oxygen radical anion with pyridine

Lixia Wu, Feng Yu, Lei Song, Xiaoguo Zhou *, Shilin Liu

Hefei National Laboratory for Physical Sciences at the Microscale, Department of Chemical Physics, University of Science and Technology of China, Hefei, Anhui 230026, PR China

ARTICLE INFO

Article history:
Received 9 April 2010
Received in revised form 12 July 2010
Accepted 22 July 2010
Available online 27 July 2010

Keywords:
Atomic oxygen radical anion (O^-)
Pyridine (C_5H_5N)
Reaction mechanism
Reaction enthalpy

ABSTRACT

The reaction mechanism of atomic oxygen radical anion (O^-) with pyridine (C_5H_5N) has been investigated at the G3MP2B3 level of theory. Three different entrance potential energy surfaces are explored, respectively, as atomic oxygen radical anion attacks γ-, β- and α-H atoms of pyridine. Possible thermodynamic product channels are examined subsequently. Based on the calculated G3MP2B3 energies and optimized geometries of all species for the title reaction, it has been demonstrated that the oxide anion formation channel is dominant, and the $C_5H_3N^- + H_2O$ channel is also favorable in thermodynamics, whereas the H-abstraction and H^+-abstraction channels are inaccessible at room temperature. The present conclusions are consistent qualitatively with the previous experimental results. The secondary reactions of the anionic products are expected to be responsible for the contradiction of branching ratios between present calculation and previous experiments.

1. Introduction

The atomic oxygen radical anion (O^-) is one of the most active anions [1,2], and can react rapidly with most molecules. The ion–molecule reactions involving the O^- anion have stimulated a variety of studies in many fields, such as ionospheric chemistry, combustion chemistry, catalytic chemistry, negative ion chemical ionization mass spectrometry (NICI-MS) [3–7]. More importantly, such ion–molecule reactions have been widely used to synthesize various anions of the classical intermediates in organic chemistry [1,8]. For instance, *o*-benzyne radical anion (*o*-$C_6H_4^-$) is produced in the reaction of O^- with benzene [9,10], and vinylidene anion ($CH_2{=}C^-$) is formed in the reaction of O^- and ethylene [11]. Therefore, it is necessary to investigate these reactions extensively for atmospheric chemistry, radiation chemistry, organic and biologic chemistry. Moreover, these reactions will give insights into syntheses of organic intermediate anions and mechanisms of liquid-phase chemical reactions.

Pyridine (C_5H_5N) is one of the most important six-membered heterocyclic compounds, which can be seen as resulting from a nitrogen atom replacing one CH group in benzene molecule. Thus the reaction mechanism of O^- with pyridine should be similar to that of O^- with benzene [12,13], and several interesting anions are expected to be produced in this reaction, like $C_5H_4NO^-$ and $C_5H_3N^-$. However, as far as we know, only a few experimental studies of the reaction between O^- with pyridine have been done, and the related thermochemical data are unavailable. The possible reaction pathways of O^- with pyridine in thermodynamics are listed as follows:

$$O^- + C_5H_5N \rightarrow C_5H_4NO^- + H, \quad \text{oxide anion formation} \tag{1}$$
$$\rightarrow C_5H_3N^- + H_2O, \quad H_2^+\text{-abstraction} \tag{2}$$
$$\rightarrow C_5H_4N + OH^-, \quad \text{H-abstraction} \tag{3}$$
$$\rightarrow C_5H_4N^- + OH. \quad H^+\text{-abstraction} \tag{4}$$

Guo and Grabowski [14] applied the flowing afterglow (FA) technique to study the reaction of O^- with pyridine, and only two anionic products, $C_5H_3N^-$ and $C_5H_4NO^-$ were detected. The corresponding branching ratios were: $C_5H_3N^- + H_2O$ 46%, $C_5H_4NO^- + H$ 54%. Anionic products of the reaction of O^- with perdeuterated pyridine (C_5D_5N) were measured as well, and similar branching ratios were reported: $C_5D_3N^- + D_2O$ 38%, and $C_5D_4NO^- + D$ 62%. Bruins et al. [15] studied the title reaction in a double-focusing mass spectrometer, and found that the $C_5H_4NO^-$ anion was the dominant ionic product, along with a prominent peak of $C_5H_3N^-$ and a low intensity peak corresponding to $C_5H_4N^-$ in mass spectra. It was a pity that no branching ratios for these anionic products were measured.

The previous experiments can only offer a little information about anionic product channels, and a clear reaction mechanism is very difficult to be deduced from the detected anionic products. More significantly, some secondary reactions of the anionic products are probably involved in the previous experiments, which could cause contamination of the measured anions, as suggested

* Corresponding author. Tel.: +86 551 3600031; fax: +86 551 3602323.
E-mail address: xzhou@ustc.edu.cn (X. Zhou).

0166-1280/$ - see front matter © 2010 Elsevier B.V. All rights reserved.
doi:10.1016/j.theochem.2010.07.032

in Ref. [1], e.g. the OH^- can react rapidly with the pyridine. Therefore, high-level theoretical calculations are necessary to clarify reaction mechanisms, since the theoretical calculations are believed to be more powerful to describe details of reaction processes.

To our knowledge, no such theoretical study has been performed for this title reaction yet. In this work, density-function theory (DFT) is applied to explore the reaction potential energy surfaces (PESs) of O^- with pyridine. The molecular structures of all species are optimized, and the possible thermodynamic reaction pathways are examined in detail. Based on our calculations, the formation mechanisms for those anions detected in the previous experiments will be presented, and the favorable product channels will be identified. Additionally, a lot of useful information will be provided for further study of the reactions of O^- with heterocyclic compounds, through comparing mechanisms of the title reaction and the reaction of $O^- + C_6H_6$.

2. Computational methods

All calculations were carried out using the Gaussian 03 program package [16]. The DFT-B3LYP method [17,18] and G3MP2B3 high-level energy calculations [19] were applied to study the reaction of O^- with pyridine, as the previous studies [20–23] showed that these methods performed well to deal with open-shell reaction systems with one negative charge. Geometries of reactants, products, intermediates (denoted as IMs) and transition states (denoted as TSs) were optimized at the B3LYP level with the 6-31+G(d,p) basis set, and the harmonic vibrational frequencies and zero point energies (ZPEs) (scaled by 0.96 [19]) were calculated at the same level. In order to reveal the influence of different basis sets on the molecular geometries, the 6-311++G(d,p) basis set was also used to re-optimize the key species. Mass-weighted intrinsic reaction coordinate (IRC) calculations [24,25] were performed for the transition states to identify the corresponding reactants and products. Meanwhile, Mulliken charge population analysis [26] was employed to reveal charge transfers during the reaction process. To obtain high-precision energy, the G3MP2B3 method was performed to calculate the single-point energies, relative energies of all key species and reaction enthalpies of the corresponding production channels. In the present G3MP2B3 calculations, the projected MP2 (PMP2) [27–29] energies were used to replace the UMP2 energies to avoid the spin contamination effect. In addition, the standard 6-31G(d) basis set in the B3LYP optimization step of G3MP2B3 method was substituted by the 6-31+G(d,p) basis set to involve the possible diffuse electron effect on the title reaction system. In order to insure the reliability of our G3MP2B3 energies, the B3PW91 [30], B3P86 [31] and ROMP2 [32,33] methods with the large basis set aug-cc-pVTZ [34] were employed as well to calculate the barrier heights of the oxide anion formation channel (1) and the H_2^+-abstraction channel (2).

3. Results and discussions

The B3LYP optimized geometry of pyridine is shown in Fig. 1, where Mulliken charge populations of each H atom is presented as well. Due to the π-bond conjugate in pyridine, the heterocycle is partially electronegative, whereas the hydrogen atoms are partially electropositive. As a result of the charge induction effect, the electropositive H atom is strongly attracted by O^- to form initial intermediate when O^- approaches pyridine. Since there are three different types of hydrogen atoms in a pyridine molecule: one γ-H, two β-H and two α-H atoms, three corresponding initial reaction intermediates are expected to form. On the basis of this assumption, three different reaction PESs of O^- with pyridine are studied separately using the B3LYP method. In present calculations, there are no obvious differences in the optimized geometries with the 6-31+G(d,p) and 6-311++G(d,p) basis sets. In the following sections, the B3LYP/6-31+G(d,p) geometries and the G3MP2B3 energies are used unless otherwise noted.

3.1. Oxide anion formation channel (1)

For the cases of O^- attacking the γ-H or β-H of pyridine, an initial intermediate is located, respectively, on the entrance PES. The optimized geometries of these two intermediates are presented in Fig. 1 as well, where IM1 corresponds to that of O^- attacking the γ-H, and IM2 is related to β-H. However, when O^- approaches α-H of pyridine, no stable initial intermediate has been located on the entrance PES at the B3LYP level because of the strong charge repulsion between the lone pair of electrons of the nitrogen atom and the O^- anion. But to our surprise, two transition states (TS11 and TS9) of isomerization from IM2 have been found successfully, which correspond, respectively, to the processes of O^- approaching α-H and α-C. That means, all expected reaction processes and final production channels related to α-H can process through an isomerization from IM2. Additionally, the overall reaction mechanisms related to the γ-, β- and α-H atoms of pyridine are very similar, and thus we will mainly describe the case of O^- attacking the γ-H in the following sections.

3.1.1. The case of O^- attacking the γ-H of pyridine

When O^- attacks the γ-H of pyridine at the initial reaction stage, IM1 (with C_{2v} symmetry) will be formed. As shown in Fig. 1, the active C–H bond length in IM1 is elongated a bit to 1.108 Å and the distance between γ-H atom and O^- is 1.665 Å, which is slightly shorter than a normal hydrogen bond length. Since IM1 has an energy of

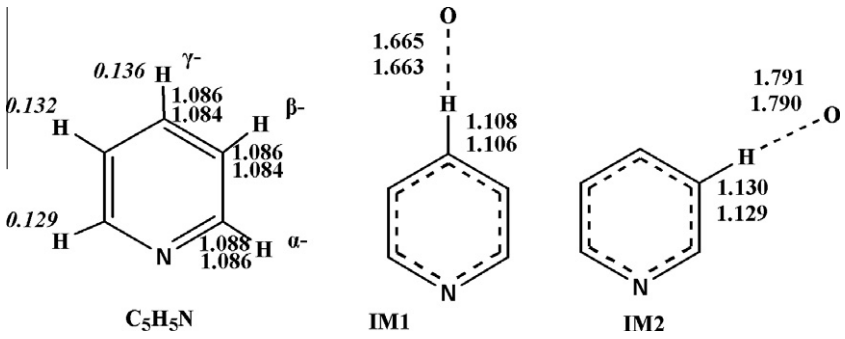

Fig. 1. The B3LYP optimized geometries of pyridine and two entrance intermediates, where the upper and lower parameters are obtained with 6-31+G(d,p) and 6-311++G(d,p) basis sets, respectively. Mulliken charge populations of every H atoms in pyridine are presented in italics as well. Bond lengths are in Angstrom, and bond angles are in degree.

72.2 kJ mol^{-1} lower than the initial reactants, it can easily further decompose or isomerize to various final products.

The B3LYP optimized geometries of those key stationary points on the reaction PES of channel (1) are shown in Fig. 2, where the imaginary vibration modes of transition states are also presented. The G3MP2B3 energies, relative energies and reaction enthalpies of these species are listed in Table 1.

The overall reaction process to produce the oxide anion in the case of O^- attacking the γ-H can be represented as the following scheme.

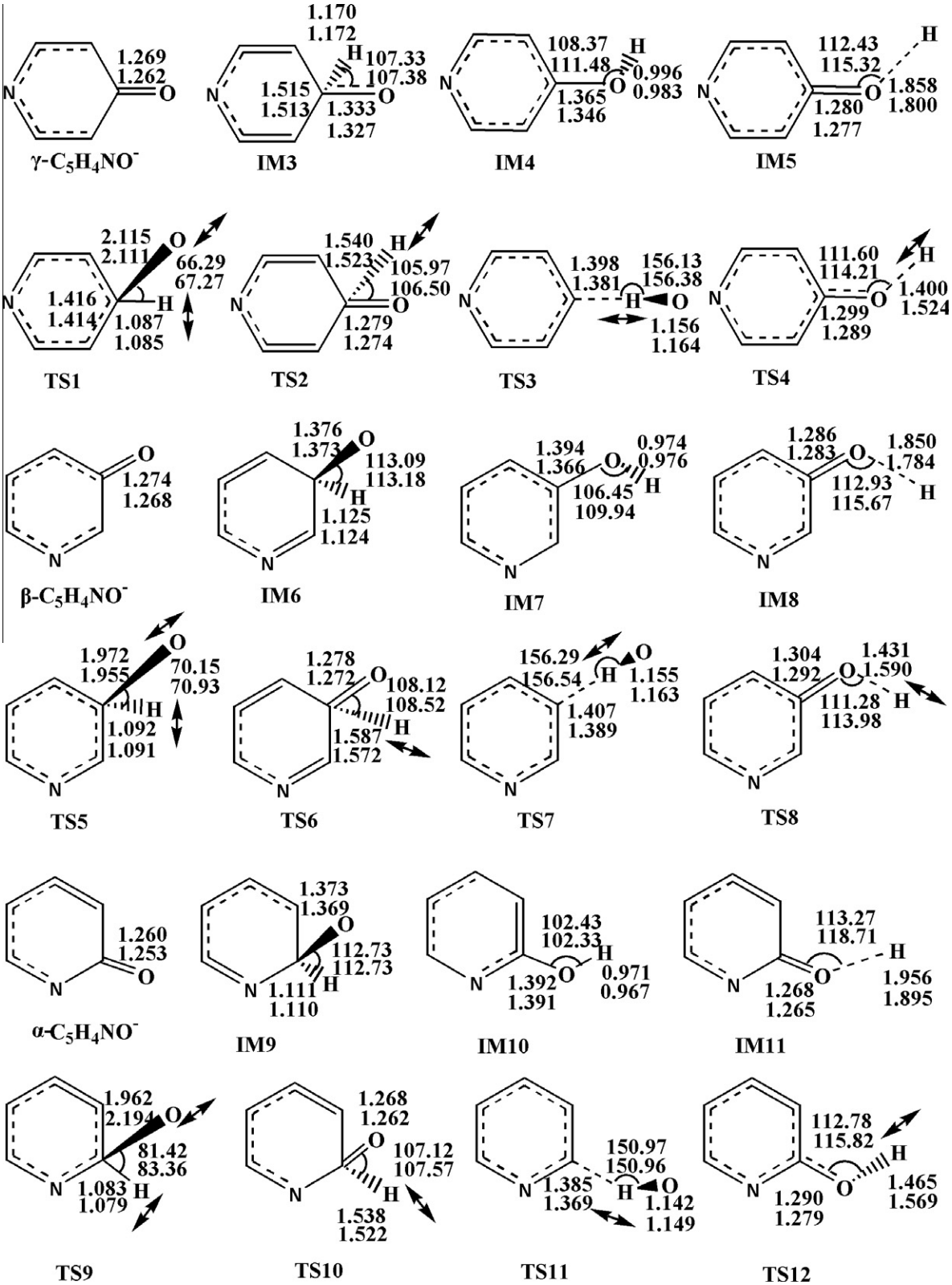

Fig. 2. The B3LYP optimized geometries of the key stationary points on the reaction PES of channel (1), where the upper and lower parameters are obtained with 6-31+G(d,p) and 6-311++G(d,p), respectively. Bond lengths are in Angstrom, and bond angles are in degree.

Table 1
Total energies, relative energies and ZPEs of key species at 0 K, and reaction enthalpies at 298 K, for the oxide anion formation channel (1).

Species	ν_i (cm^{-1})[a]	ZPE (hartree)[b]	E_0[G3MP2B3] (hartree)	ΔE (kJ mol^{-1})	ΔrH_{298} (kJ mol^{-1})
$C_5H_5N + O^-$		0.08518	−322.92168	0.0	0.0
γ-$C_5H_4NO^-$ + H		0.07639	−322.99716	−198.2	−196.1
β-$C_5H_4NO^-$ + H		0.07590	−322.98710	−171.8	−169.6
α-$C_5H_4NO^-$ + H		0.07588	−322.99392	−189.7	−187.4
IM1		0.08744	−322.94919	−72.2	
IM2		0.08401	−322.95308	−82.4	
IM3		0.08235	−322.97736	−146.2	
IM4		0.08419	−323.01916	−255.9	
IM5		0.07890	−322.99855	−201.8	
IM6		0.08345	−322.98116	−156.2	
IM7		0.08369	−323.01223	−237.7	
IM8		0.07844	−322.98889	−176.4	
IM9		0.08449	−322.97875	−149.8	
IM10		0.08384	−323.02198	−263.3	
IM11		0.07790	−322.99527	−193.2	
TS1	205*i*	0.08389	−322.93742	−41.3	
TS2	980*i*	0.07815	−322.97736	−146.2	
TS3	1055*i*	0.07767	−322.93228	−27.8	
TS4	979*i*	0.07866	−322.99806	−200.5	
TS5	302*i*	0.08368	−322.93524	−35.6	
TS6	917*i*	0.07762	−322.97103	−129.6	
TS7	1049*i*	0.07775	−322.92928	−19.9	
TS8	892*i*	0.07812	−322.98934	−177.6	
TS9	392*i*	0.08508	−322.92830	−17.4	
TS10	958*i*	0.07778	−322.97356	−136.2	
TS11	1173*i*	0.07720	−322.93414	−32.7	
TS12	842*i*	0.07738	−322.99335	−188.2	

[a] Calculated at the B3LYP/6-31+G(d,p) level.
[b] ZPEs are calculated with the vibrational frequencies scaled by 0.96 [19].

$$O^- + C_5H_5N \rightarrow IM1 \begin{cases} \xrightarrow{TS1} IM3 \xrightarrow{TS2} \gamma\text{-}C_5H_4NO^- + H \\ \xrightarrow{TS3} IM4 \xrightarrow{TS4} IM5 \rightarrow \gamma\text{-}C_5H_4NO^- + H \end{cases} \quad (5)$$

Obviously, the oxide anion formation products, γ-$C_5H_4NO^-$ + H, can be produced from IM1 through two possible pathways. The more favorable pathway can be described as an isomerization-decomposition process. IM1 firstly isomerizes to IM3 via a transition state TS1. In this process, O^- approaches the active C atom from out of ring plane, the γ-H atom connected to the heterocycle is pushed out of plane and the single C–O bond is formed gradually. TS1 has a barrier height of 30.9 kJ mol^{-1} compared with IM1, but is still lower than the initial reactants in energy. In IM3, the distance between the C and O atoms is rapidly shortened from 2.115 Å in TS1 to 1.333 Å, and both C–C bonds involving the active C atom in the heterocycle are elongated from 1.416 Å in TS1 to 1.515 Å. Moreover, the active C atom in IM3 is changed from sp^2 to sp^3 hybrid, and the original conjugate π-bond structure in the heterocycle is broken. Thus, IM3 has a tendency to break the active C–H bond and reform a conjugate π-bond structure in the heterocycle. As IM3 has an energy of 146.2 kJ mol^{-1} lower than the reactants, it can easily overcome the dissociation barrier TS2 to produce γ-$C_5H_4NO^-$ anion. As shown in Fig. 2, the C–H bond in TS2 is significantly elongated to 1.540 Å and the C–O distance is shortened to a typical double bond length 1.279 Å. Briefly, the structure of C_5H_4NO moiety in TS2 is very close to that of the γ-$C_5H_4NO^-$ anion, indicating TS2 is a late barrier.

As indicated in the scheme (5), the γ-$C_5H_4NO^-$ anion can also be formed via another isomerization-decomposition process of IM1. In fact, the isomerization process from IM1 to IM4 looks like a typical atom-insertion reaction process [35,36]. As the C–H bond of IM1 breaks and the γ-H atom moves away from the heterocycle, the O^- anion deviates from the heterocycle plane gradually and then rapidly attaches to the active C to form the C–O bond, and IM4 is produced finally. Mulliken charge population analysis shows that the negative charges on the O atom of IM1 and IM4 are −0.817 and −0.104, respectively, implying that the negative charge on the O atom has almost all transferred to the heterocycle in this process. Actually, as the pyridine is electron deficient, it favors electron transfer from the O atom to the heterocycle to form the conjugation between the *p*-orbital of the O atom and the π-bond of the heterocycle in IM4, and thus the molecular system becomes more stable.

IM4 is substantially lower in energy than the initial reactants, and is facile to further dissociate to γ-$C_5H_4NO^-$ and H atom through a barrier TS4. The O–H bond in TS4 is significantly elongated to 1.400 Å, and the C=O double bond is formed. An ion–dipole intermediate IM5 has been located on the exit PES, in which the O–H distance length has increased to 1.858 Å. As a typical product-like intermediate γ-$C_5H_4NO^-\cdots$H, IM5 can finally decompose to products, γ-$C_5H_4NO^-$ and H.

For the two aforementioned reaction pathways to produce γ-$C_5H_4NO^-$ + H, the energies of the two rate-controlling barriers, TS1 and TS3, are both lower than that of the initial reactants. Thus the oxide formation channel is favorable to happen, and the overall exothermic energy is 198.2 kJ mol^{-1}. The first pathway, O^- + C_5H_5N → IM1 → IM3 → γ-$C_5H_4NO^-$ + H, should be dominant owing to its lower rate-controlling step barrier TS1.

3.1.2. The case of O^- attacking the β- and α-H of pyridine

When O^- attacks the β- or α-H of pyridine, a unique initial ion–dipole intermediate IM2 will be formed with C_s symmetry on the entrance PES. As mentioned above, two transition states (TS11 and TS9) have been found to correspond, respectively, to the subsequent processes of O^- approaching α-H and α-C, and thus the production channels (1-4) related to α- position of pyridine will follow. As shown in Fig. 2, the imaginary vibration movement of TS11 actually corresponds to the α-H abstraction process, while the imaginary vibration mode of TS9 corresponds to the approaching of O^- towards α-C atom and the α-H rocking out of the heterocycle plane. In other words, TS11 and TS9 look like the initial transition states of the H-abstraction and oxide anion formation

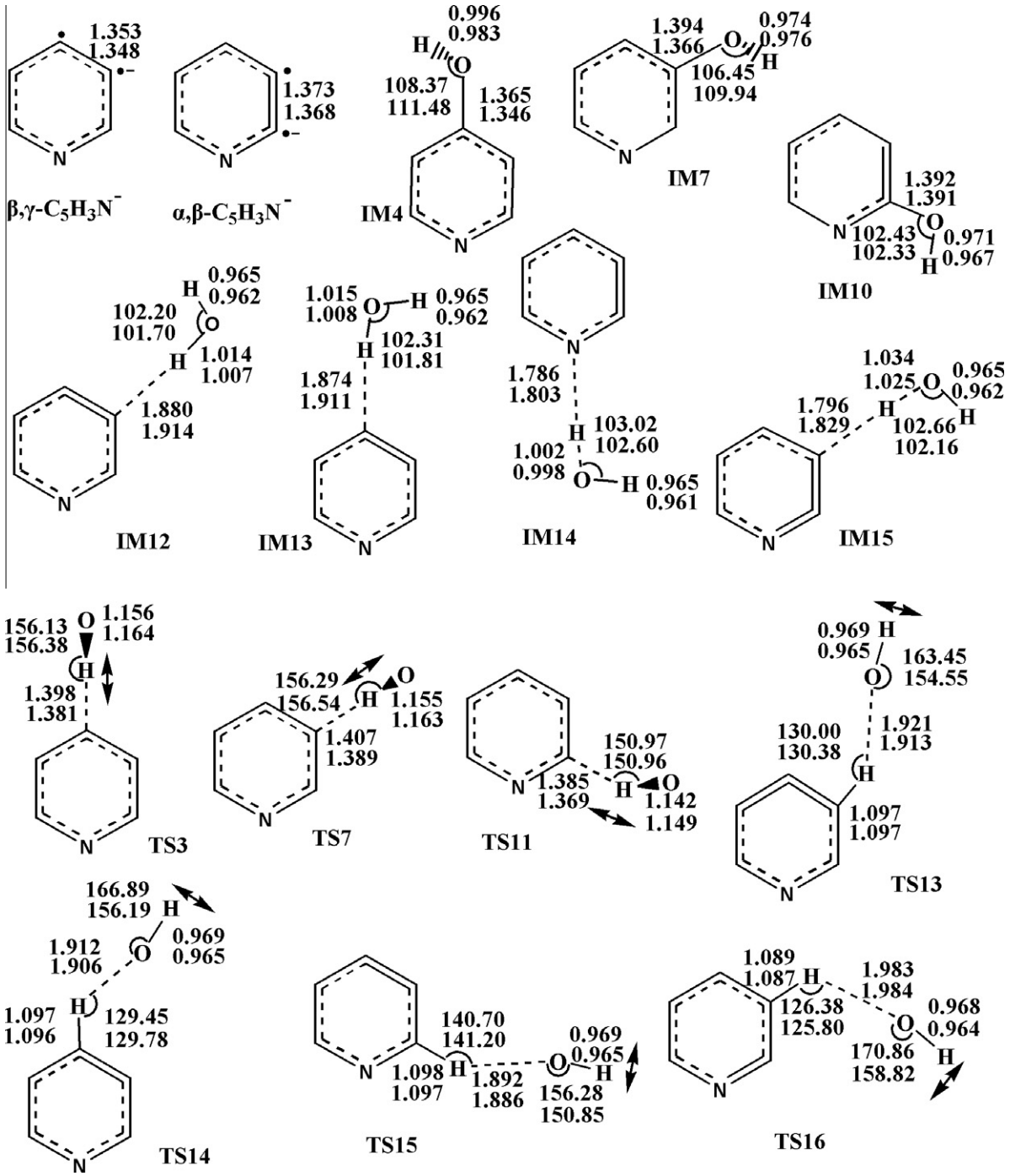

Fig. 3. The B3LYP optimized geometries of the key stationary points on the reaction PES of channel (2), where the upper and lower parameters are obtained with 6-31+G(d,p) and 6-311++G(d,p), respectively. Bond lengths are in Angstrom, and bond angles are in degree.

channels, respectively. Very interestingly, our reverse IRC calculations for TS11 and TS9 point to the same unexpected intermediate IM2, which is indeed an entrance intermediate complex formed by O^- attacking β-H. That means, the lone pair electrons of the nitrogen atom effectively hinder O^- from approaching the α-H atom to form a stable initial intermediate, and all subsequent reaction processes related with the α-H or α-C atoms of pyridine are originated from IM2 in fact. The forward IRC calculations for TS11 and TS9 point to IM10 and IM9, respectively, in both of which the active carbon atom is the α-C atom. Thus we still identify the subsequent reaction processes as the reaction pathways induced by O^- attacking α-H of pyridine, in order to be distinguished from the aforementioned reaction mechanism of O^- attacking β-H. As an example, the relative energy diagram for the static reaction pathway involving TS11 on the entrance PES is shown in Fig. S1 of Supplementary materials.

The subsequent oxide anion formation channels can be accomplished through the isomerization and decomposition of IM2, as shown in the following schemes.

$$O^- + C_5H_5N \rightarrow IM2 \begin{cases} \xrightarrow{TS5} IM6 \xrightarrow{TS6} \beta\text{-}C_5H_4NO^- + H \\ \xrightarrow{TS7} IM7 \xrightarrow{TS8} IM8 \rightarrow \beta\text{-}C_5H_4NO^- + H \end{cases} \quad (6)$$

Table 2
Total energies, relative energies and ZPEs of key species at 0 K, and reaction enthalpies at 298 K, for the H_2^+-abstraction channel (2).

Species	v_i (cm^{-1})[a]	ZPE (hartree)[b]	E_0[G3MP2B3] (hartree)	ΔE (kJ mol^{-1})	ΔrH_{298} (kJ mol^{-1})
$C_5H_5N + O^-$		0.08518	−322.92168	0.0	0.0
β,γ-$C_5H_3N^- + H_2O$		0.07978	−322.95268	−81.4	−77.5
α,β-$C_5H_3N^- + H_2O$		0.07920	−322.93952	−46.8	−42.9
IM1		0.08744	−322.94919	−72.2	
IM2		0.08401	−322.95308	−82.4	
IM4		0.08419	−323.01916	−255.9	
IM7		0.08369	−323.01223	−237.7	
IM10		0.08384	−323.02198	−263.3	
IM12		0.08195	−322.96884	−123.8	
IM13		0.08202	−322.96899	−124.2	
IM14		0.08222	−322.95915	−98.4	
IM15		0.08127	−322.96366	−110.2	
TS3	1055*i*	0.07767	−322.93228	−27.8	
TS7	1049*i*	0.07775	−322.92928	−19.9	
TS11	1173*i*	0.07720	−322.93414	−32.7	
TS13	139*i*	0.08138	−322.94429	−59.4	
TS14	143*i*	0.08155	−322.94329	−56.7	
TS15	110*i*	0.08114	−322.93716	−40.6	
TS16	117*i*	0.08107	−322.94521	−61.8	

[a] Calculated at the B3LYP/6-31+G(d,p) level.
[b] ZPEs are calculated with the vibrational frequencies scaled by 0.96 [19].

$$O^- + C_5H_5N \rightarrow IM2 \begin{cases} \xrightarrow{TS9} IM9 \xrightarrow{TS10} \alpha\text{-}C_5H_4NO^- + H \\ \xrightarrow{TS11} IM10 \xrightarrow{TS12} IM11 \rightarrow \alpha\text{-}C_5H_4NO^- + H \end{cases} \quad (7)$$

The scheme (6) and (7) are related to the cases of O^- attacks the β- and α-H, respectively. The optimized geometries of the key species involved in these schemes are shown in Fig. 2 as well. The G3MP2B3 energies, relative energies and reaction enthalpies of these species are also summarized in Table 1.

As the overall reaction mechanism is similar to that of O^- attacking the γ-H, we just give brief descriptions of these product channels here. In scheme (6), the overall reaction process to produce β-$C_5H_4NO^-$ anion is still exothermic by 171.8 kJ mol^{-1} and all barriers involved are lower than the initial reactants in energy. The rate-controlling barriers for these two pathways are TS5 and TS7, whose heights are 46.8 and 62.5 kJ mol^{-1}, respectively. Due to a lower rate-controlling barrier, the pathway $O^- + C_5H_5N \rightarrow IM2 \rightarrow IM6 \rightarrow$ β-$C_5H_4NO^-$ + H, is more favorable. The scheme (7) is very similar to the scheme (6). Both IM10 and IM9 are formed through exothermic reaction processes and can easily overcome the subsequent isomerization and dissociation barriers. The overall reaction process is exothermic by 189.7 kJ mol^{-1}. In the two pathways to produce α-$C_5H_4NO^-$ anion, the rate-controlling barriers are TS11 and TS9, and the barrier heights are 49.7 and 65.0 kJ mol^{-1}, respectively. Therefore, the latter pathway, $O^- + C_5H_5N \rightarrow IM2 \rightarrow IM10 \rightarrow IM11 \rightarrow$ α-$C_5H_4NO^-$ + H, is more favorable.

3.2. H_2^+-abstraction channel (2)

As previous studies have shown [1], the H_2^+-abstraction process is another important reaction channel in the reactions of O^- with molecules containing hydrogen atoms. In the title reaction, the H_2O molecule can be produced from IM1 or IM2 via the following multi-steps schemes:

$$O^- + C_5H_5N \rightarrow IM1 \xrightarrow{TS3} IM4 \xrightarrow{TS13} IM12 \rightarrow \beta,\gamma\text{-}C_5H_3N^- + H_2O \quad (8)$$

$$O^- + C_5H_5N \rightarrow IM2 \xrightarrow{IM7} \begin{cases} \xrightarrow{TS14} IM13 \rightarrow \beta,\gamma\text{-}C_5H_3N^- + H_2O \\ \xrightarrow{TS15} IM14 \rightarrow \alpha,\beta\text{-}C_5H_3N^- + H_2O \end{cases} \quad (9)$$

$$O^- + C_5H_5N \rightarrow IM2 \xrightarrow{TS11} IM10 \xrightarrow{TS16} IM15 \rightarrow \alpha,\beta\text{-}C_5H_3N^- + H_2O \quad (10)$$

The schemes (8-10) correspond to the reaction cases of O^- approaching the γ-, β- and α-H atoms of pyridine. The B3LYP optimized geometries of these key stationary points on the reaction PES of channel (2) are shown in Fig. 3, where the imaginary vibration modes of transition states are also presented. The G3MP2B3 energies, relative energies and reaction enthalpies of the species are listed in Table 2.

In the overall reaction processes, the first isomerization steps from IM1 to IM4, IM2 to IM7 and IM2 to IM10, are the rate-determining steps for the H_2^+-abstraction channel (2), respectively. In these isomerization processes, the OH group leaves from the heterocycle and approaches the neighboring H atom gradually. A new ion–dipole intermediate, $C_5H_3N^-\cdots H_2O$, is formed finally. Although the barrier energies involved is much higher than that of the entrance intermediates, IM1 or IM2, the overall H_2^+-abstraction reaction is still energetically allowed. As shown in Table 2, the exothermic energies are 81.4 kJ mol^{-1} for producing β,γ-$C_5H_3N^-$ + H_2O, and 46.8 kJ mol^{-1} for producing α,β-$C_5H_3N^-$ + H_2O.

In order to compare all production pathways and identify the dominant channel, the schematic diagrams of the G3MP2B3 relative energies of various species on the reaction PES are shown in Fig. 4, in which Fig. 4a, b and c present the reaction mechanism of O^- attacking γ-, β- and α-H atom of pyridine, respectively.

As indicated in Fig. 4, the H_2^+-abstraction channel (2) and oxide anion formation channel (1) can come from the same intermediate, but the subsequent barrier height of channel (2) is much higher than that of channel (1). Therefore, the H_2^+-abstraction channel (2) is relatively less important than the oxide anion formation channel (1).

3.3. H-abstraction channel (3) and H^+-abstraction channel (4)

The H-abstraction channel (3) and H^+-abstraction channel (4) need an O^- insertion process to subsequently proceed. As mentioned above, three energetic intermediates are formed via the typical atom-insertion process, e.g. IM4 for γ-position reaction, IM7 for β- and IM10 for α- position. These intermediates can decompose directly by breaking the C–O bond, and two possible decomposition products are obtained: one is $C_5H_4N + OH^-$ (H-abstraction channel (3)), and the other is $C_5H_4N^-$ + OH (H^+-abstraction channel (4)). The corresponding G3MP2B3 energies, relative energies and reaction enthalpies for these two channels are listed in Table 3, and the B3LYP optimized geometries of C_5H_4N and $C_5H_4N^-$ in-

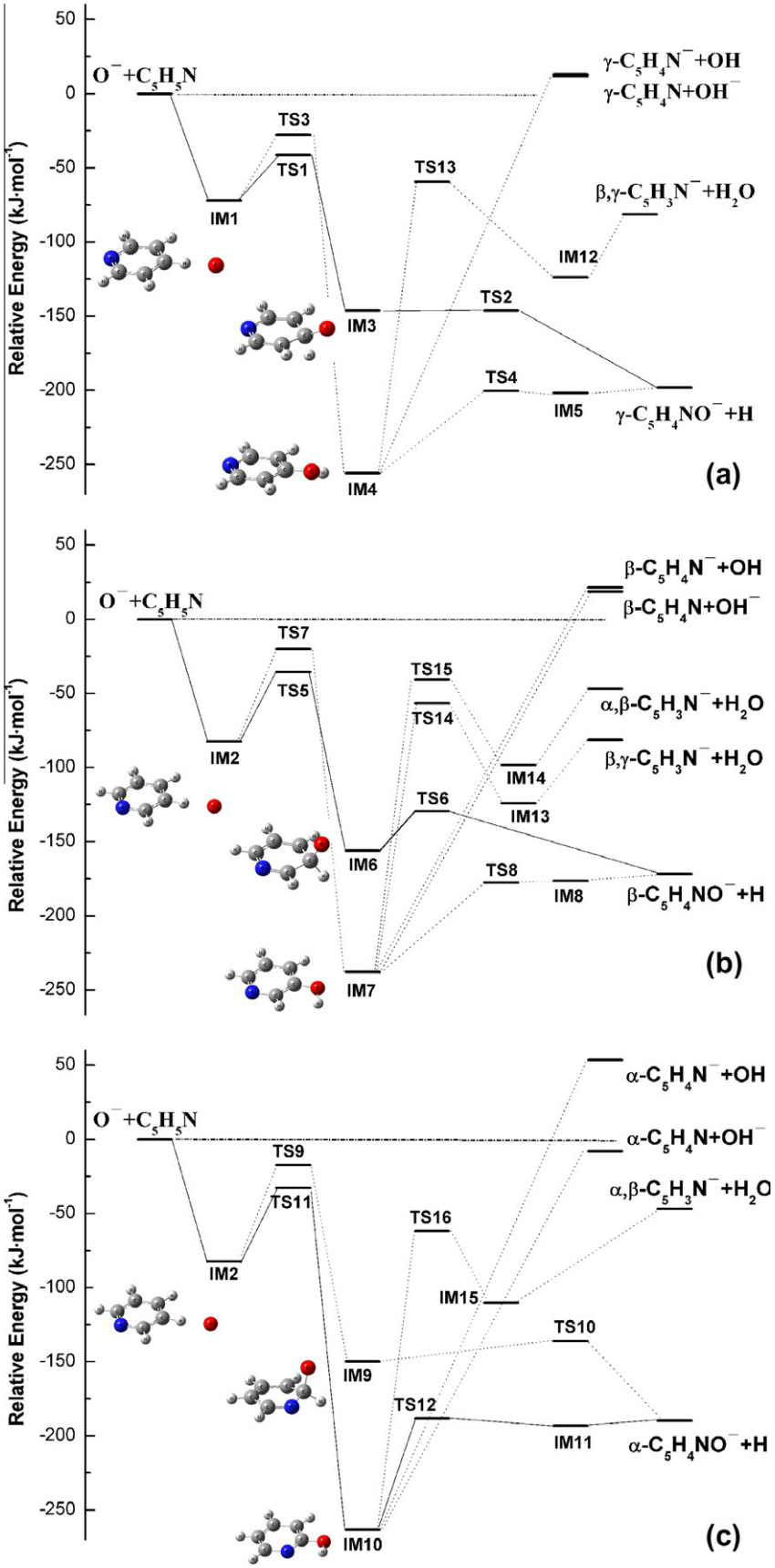

Fig. 4. Schematic diagram of the G3MP2B3 relative energies of various species on the reaction PES. (a) O^- attacks the γ-H atom of pyridine; (b) O^- attacks the β-H; (c) O^- attacks the α-H atom.

Table 3
Total energies, relative energies and ZPEs of key species at 0 K, and reaction enthalpies at 298 K for the H-abstraction channel (3) and H^+-abstraction channel (4).

Species	v_i (cm^{-1})[a]	ZPE (hartree)[b]	E_0[G3MP2B3] (hartree)	ΔE (kJ mol^{-1})	ΔrH_{298} (kJ mol^{-1})
$C_5H_5N + O^-$		0.08518	−322.92168	0.0	0.0
γ-$C_5H_4N^-$ + OH		0.07916	−322.91669	13.1	15.6
γ-C_5H_4N + OH^-		0.08065	−322.91718	11.8	14.3
β-$C_5H_4N^-$ + OH		0.07917	−322.91346	21.6	24.2
β-C_5H_4N + OH^-		0.08086	322.91457	18.7	21.1
α-$C_5H_4N^-$ + OH		0.07832	−322.90132	53.5	56.4
α-C_5H_4N + OH^-		0.08098	−322.92472	−8.0	−5.5
IM1		0.08744	−322.94919	−72.2	
IM2		0.08401	−322.95308	−82.4	
IM4		0.08419	−323.01916	−255.9	
IM7		0.08369	−323.01223	−237.7	
IM10		0.08384	−323.02198	−263.3	
TS3	1055*i*	0.07767	−322.93228	−27.8	
TS7	1049*i*	0.07775	−322.92928	−19.9	
TS11	1173*i*	0.07720	−322.93414	−32.7	

[a] Calculated at the B3LYP/6-31+G(d,p) level.
[b] ZPEs are calculated with the vibrational frequencies scaled by 0.96 [19].

volved in channel (3) and (4) are shown in Fig. S2 of Supplementary materials.

To locate the transition states for these channels, the relaxed potential energy scan along the elongation of the C···O distance has been calculated with other coordinates optimized to monitor the changes of molecular geometry and relative energy during the C–O bond-breaking process. No barrier has been found and the relative energy of the reaction system increases gradually as the C···O distance increases. Moreover, the two reaction PESs cross with each other and can not be distinguished at the B3LYP level. Fortunately, both channels (3) and (4) are endothermic for all cases of O^- attacking the α-, β- or γ-H atom (except that the α-C_5H_4N + OH^- formation process is slightly exothermic), and therefore they should be not important relative to the oxide anion formation channel (1) and H_2^+-abstraction channel (2).

3.4. Comparison with experimental results

Although the barrier heights and reaction enthalpies of each product channel for the title reaction are slightly different in the three cases of the O^- attacking γ-, β- and α-H of pyridine, reaction mechanisms are very similar as shown in Fig. 4. The present calculations have demonstrated that the oxide anion formation channel (1) is most dominant among the four reaction channels. The H_2^+-abstraction channel (2) is also favorable in thermodynamics while the H-abstraction channel (3) and H^+-abstraction channel (4) are both inaccessible at room temperature. These conclusions agree qualitatively with the experimental results of Guo and Grabowski [14], in which only the anion products of channel (1) and channel (2) were obtained. However, the two anionic products they obtained were almost in equal quantities, which disagrees with our conclusion that oxide anion formation channel (1) is much more favorable than H_2^+-abstraction channel (2) due to its lower barrier height of the rate-controlling step.

As shown in Fig. 4, the channels (1) and (2) proceed through the same intermediate, IM4 for γ-position reaction, IM7 for β- and IM10 for α- position. Thus the contradiction of branching ratios between present calculation and previous experiment [14] has been doubted as uncertainty of the G3MP2B3 method to calculate the related barrier heights in this open-shell reaction system. To confirm the error of G3MP2B3 level, some other popular quantum chemical computational theories have been chosen to calculate the barrier heights of the rate-controlling step of channel (2) and channel (1) in the three cases of the O^- attacking γ-, β- and α-H of pyridine. Table 4 lists the calculated differences of the two rate-controlling barrier heights with G3MP2B3, B3LYP/6-31+G(d,p), B3LYP/aug-cc-pVTZ, B3PW91/aug-cc-pVTZ, B3P86/aug-cc-pVTZ and ROMP2/aug-cc-pVTZ methods, respectively. Obviously, the barrier height differences of the two channels are not distinct at all theoretical levels, and thus the present G3MP2B3 results should be reliable, indicating that more experimental investigations should be carried out to study the product branching ratios of this reaction system. It needs to be emphasized that the secondary reactions of those anionic products were probably involved in the previous experiment [14], which could cause contamination of the measured anions, as suggested in Ref. [1].

Additionally, in the mass spectra measured by Bruins et al. [15], a weak anion signal corresponding to $C_5H_4N^-$ was detected besides the $C_5H_4NO^-$ and $C_5H_3N^-$ anions. According to our calculations, H^+-abstraction channel (3) is difficult to occur, as well as H-abstraction channel (4). More importantly, the active energies for these two channels are very close in the case of O^- attacking β- and γ-H of pyridine, even while more slight active energies are needed for H^+-abstraction than H-abstraction pathway in the case of O^- attacking α-H. Therefore, the OH^- anion should exist as well as the $C_5H_4N^-$ anion when the title reaction system has a high enough initial reaction energy, which obviously disagrees with the experimental results of Bruins et al. [15]. A possible reason for explaining

Table 4
The barrier height differences of the rate-controlling steps between the H_2^+-abstraction channel (2) and the oxide anion formation channel (1) in the three cases of O^- attacking γ-, β- and α-H of pyridine.

Methods	γ-Position	β-Position		α-Position
	ΔE(TS13–TS4)	ΔE(TS14–TS8)	ΔE(TS15–TS8)	ΔE(TS16–TS12)
B3LYP/6-31+G(d,p)	110.8	92.5	107.0	101.3
B3LYP/aug-cc-pvtz	122.6	103.6	117.1	111.9
B3PW91/aug-cc-pvtz	139.7	120.0	133.6	128.0
B3P86/aug-cc-pvtz	140.8	121.2	135.4	129.1
ROMP2/aug-cc-pvtz	135.4	120.9	132.8	119.0
G3MP2B3	141.1	120.9	137.0	126.4

this disagreement is that a trace of OH^- anion exists inevitably in the preparation process of O^- source, and its secondary reactions with pyridine caused the quenching of OH^- itself and the formation of the $C_5H_4N^-$ anions. Because the proton affinity (PA) of OH^- anion is 1633 kJ mol^{-1} [37,38], which is even higher than that of the O^- anion (1601 kJ mol^{-1} [39]), it is a highly active anion and can abstract a proton of pyridine to produce the $C_5H_4N^-$ anion. The similar secondary reaction process has been confirmed to contribute to the branching ratios of anionic products in the $O^- + C_6H_6$ reaction [22].

3.5. Comparison with the reactions of $O^- + C_6H_6$ and $O^- + C_2H_4$

As shown in Fig. 4, the overall reaction processes of the title reaction is analogical to that of $O^- + C_6H_6$ [13], and the two reaction systems have similar initial ion–dipole intermediates formed on the entrance PES. Only in the case of O^- attacking α-H of pyridine, the lone pair electrons of the nitrogen atom effectively hinder O^- from approaching the α-H to form the expected initial ion–dipole intermediate. Interestingly, the subsequent reaction processes seem to undergo the expected way similar to those in the cases of the O^- attacking β- and γ-H, in which the active reaction position of heterocycle is still α-H or α-C atoms.

Since ethylene (C_2H_4) is the simplest alkene, the reaction mechanism between it with O^- is another important example for us to understand the ion–molecule interaction. As the extensive potential energy profile mapped in Ref. [22] shown, the initial stage of the $O^- + C_2H_4$ reaction is also similar, and an ion–dipole intermediate complex will be formed when O^- approaches ethylene. Among all anionic production channels, the CH_2CHO^- oxide anion formation is the most dominant due to the lowest barrier. All static production pathways are very similar between the title reaction with $O^- + C_2H_4$. Very recently, we have also explored the potential dynamic reaction pathways of the $O^- + C_2H_4$ reaction [40], compared with the static reaction mechanism revealed by IRC calculations. Interestingly, the reaction presents a few different dynamic production pathways, especially when the initial kinetic energy of reactants is relatively high. For instance, the formation of $OH^- + CH_2{=}CH$ products can depart from the minimum energy path (MEP) and bypass the deep potential well of intermediate. However, the oxide formation and H_2^+-abstraction pathways do not present any dynamic effects yet. That means, the dynamic effect would be obvious only in the direct H-atom abstraction process between O^- and organic molecule, including the title reaction of $O^- + C_5H_5N$. Since the H (or H^+) abstraction in the $O^- + C_5H_5N$ reaction is much endothermic than the oxide anion formation (1) and H_2^+-abstraction (2) channels, this kind of dynamic effect will not cause serious contamination of branching ratio of the anionic products.

4. Conclusions

G3MP2B3 method has been applied to investigate the reaction mechanism of atomic oxygen radical anion with pyridine. On the entrance reaction PES, an initial ion–dipole intermediate is located, respectively, when atomic oxygen radical anion approaches γ- and β-H atom of pyridine, but no similar intermediate has been found when O^- attacks α-H. The lone pair electrons of the nitrogen atom in the heterocycle effectively hinder O^- from approaching α-H to form the expected initial ion–dipole intermediate. Interestingly, two unexpected isomerizations involving movement of O^- from β-H to α-H or α-C can happen in this case, and thus the subsequent reaction for O^- attacking α-H can progress on the its normal way.

Four possible thermodynamic product channels are investigated systematically on the reaction PES. Geometries of all species are optimized at the B3LYP/6-31+G(d, p) level, and high-precision G3MP2 energies and reaction enthalpies are obtained subsequently. Although there are certain differences among the overall reaction processes when O^- initially attacks γ-, β- and α-H atoms, reaction mechanisms are very similar as shown in Fig. 4. Compared with the H_2^+-abstraction (2), H-abstraction (3) and H^+-abstraction (4) channels, the oxide anion formation channel (1) is dominant for its lowest barrier height. The H_2^+-abstraction channel (2) is also favorable in thermodynamics, while the H-abstraction channel (3) and H^+-abstraction channel (4) are both inaccessible at room temperature. The present conclusions are consistent qualitatively with the previous experimental results [14].

Based on our calculations, the detected $C_5H_4N^-$ anion in the experiment of Bruins et al. [15] should come from secondary reactions of the OH^- anions involved in the experiment. The secondary reaction between OH^- with pyridine would cause the quenching of the OH^- anion itself and produce the $C_5H_4N^-$ anion, because the OH^- anion is a highly active anion and it is able to fast abstract a proton of pyridine.

Acknowledgements

The financial supports from the National Natural Science Foundation of China (NSFC, Nos. 20603033 and 10979042) and National Key Basic Research Special Foundation (NKBRSF, No. 2007CB815204) are gratefully acknowledged.

Appendix A. Supplementary data

Supplementary data associated with this article can be found, in the online version, at doi:10.1016/j.theochem.2010.07.032.

References

[1] J. Lee, J.J. Grabowski, Chem. Rev. 92 (1992) 1611. and references therein.
[2] J.H. Futrel1, T.O. Tieman, Ion–molecule Reactions, vo1. 2, Lenum Press, New York, 1972.
[3] E.E. Ferguson, F.C. Fehsenfeld, D.L. Albritton, in: M.T. Bowers (Ed.), Gas Phase Ion Chemistry, vol. 1, Academic Press, New York, 1979 (Chapter 2).
[4] R.P. Wayne, Chemistry of Atmospheres, Clarendon Press, Oxford, 1985 (Chapter 6).
[5] A.B. Fialkov, Prog. Energy Combust. Sci. 23 (1997) 399.
[6] T. Dong, J. Li, F. Huang, L. Wang, J. Tu, Y. Torimoto, M. Sadakata, Q.X. Li, Chem. Commun. 21 (2005) 2724.
[7] A.G. Harrison, Chemical Ionization Mass Spectrometry, CRC Press, Boca Raton, FL, 1983.
[8] M. Born, S. Ingemann, N.M.M. Nibbering, Mass Spectrom. Rev. 16 (1997) 181.
[9] Y. Guo, J.J. Grabowski, J. Am. Chem. Soc. 113 (1991) 5923.
[10] D.G. Leopold, A.E.S. Miller, W.C. Lineberger, J. Am. Chem. Soc. 108 (1986) 1379.
[11] Y. Guo, J.J. Grabowski, Int. J. Mass Spectrom. Ion Process. 97 (1990) 253.
[12] J.A.D. Stockdale, R.N. Compton, P.W. Reinhardt, Int. J. Mass Spectom. Ion Phys. 4 (1970) 401.
[13] Y. Zhao, X. Zhou, F. Yu, J. Dai, S. Liu, Acta Phys. Chim. Sinica 22 (2006) 1095.
[14] Y. Guo, J.J. Grabowski, Int. J. Mass Spectrom. Ion. Process. 117 (1992) 299.
[15] A.P. Bruins, A.J. Correia, A.G. Harrison, K.R. Jennings, R.K. Mitchum, Adv. Mass. Spectrom. 7 (1978) 355.
[16] M.J. Frisch, G.W. Trucks, H.B. Schlegel, et al., Gaussian 03 (Revision B. 05.), Gaussian Inc., Pittsburgh, PA, 2003.
[17] C. Lee, W. Yang, R.G. Parr, Phys. Rev. B 37 (1988) 785.
[18] A.D. Becke, J. Chem. Phys. 98 (1993) 5648.
[19] A.G. Baboul, L.A. Curtiss, P.C. Redfern, K. Raghavachari, J. Chem. Phys. 110 (1999) 7650.
[20] F. Yu, Y. Zhao, Y. Wang, X. Zhou, S. Liu, Acta Chim. Sinica 65 (2007) 899.
[21] X. Wang, F. Yu, D. Xie, S. Liu, X. Zhou, Acta Chim. Sinica 66 (2008) 2499.
[22] J. Wang, F. Yu, J. Liu, S. Liu, X. Zhou, Acta Phys. Chim. Sinica 24 (2008) 1393.
[23] F. Yu, L. Wu, S. Liu, X. Zhou, J. Mol. Struc. THEOCHEM 947 (2010) 1.
[24] C. Gonzalez, H.B. Schlegel, J. Chem. Phys. 90 (1989) 2154.
[25] C. Gonzalez, H.B. Schlegel, J. Phys. Chem. 94 (1990) 5523.
[26] R.S. Mulliken, J. Chem. Phys. 23 (1955) 1833.
[27] H.B. Schlegel, J. Chem. Phys. 84 (1986) 4530.
[28] C. Sosa, H.B. Schlegel, Int. J. Quantum Chem. 29 (1986) 1001.
[29] C. Sosa, H.B. Schlegel, Int. J. Quantum Chem. 30 (1986) 155.
[30] J.P. Perdew, Y. Wang, Phys. Rev. B 45 (1992) 13244.
[31] J.P. Perdew, Phys. Rev. B 33 (1986) 8822.
[32] M.J. Frisch, M. Head-Gordon, J.A. Pople, Chem. Phys. Lett. 166 (1990) 281.

[33] R. McWeeny, G. Diercksen, J. Chem. Phys. 49 (1968) 4852.
[34] R.A. Kendall, T.H. Dunning, R.J. Harrison, J. Chem. Phys. 96 (1992) 6796.
[35] X. Zhou, S. Yu, J. Li, Z. Sheng, L. Zhang, X. Ma, Chem. Phys. Lett. 339 (2001) 117.
[36] X. Zhou, L. Pei, L. Zhang, J. Dai, Y. Chen, S. Yu, X. Ma, Chem. Phys. 279 (2002) 15.
[37] J.R. Smith, J.B. Kim, W.C. Lineberger, Phys. Rev. A 55 (1997) 2036.
[38] P.A. Schulz, R.D. Mead, P.L. Jones, W.C. Lineberger, J. Chem. Phys. 77 (1982) 1153.
[39] D.M. Neumark, K.R. Lykke, T. Andersen, W.C. Lineberger, Phys. Rev. A 32 (1985) 1890.
[40] F. Yu, L.X. Wu, L. Song, X.G. Zhou, S.L. Liu, J. Mol. Struc. THEOCHEM 958 (2010) 41.